Robert Müller, Janna Kuchinka and Thomas Heinze*

Studies about the design of magnetic bionanocomposite

Abstract: Magnetic nanocomposites are a class of smart materials that have attracted recent interest as drug delivery systems or as medical implants. A new approach toward the biocompatible nanocomposites suitable for remote melting is presented. It is shown that magnetite nanoparticles (MNPs) can be embedded into a matrix of biocompatible thermoplastic dextran esters. For that purpose, fatty acid esters of dextran with adjustable melting points in the range of 30–140 °C were synthesized. Esterification of the polysaccharide by activation of the acid as iminium chlorides guaranteed mild reaction conditions leading to high-quality products as confirmed by Fourier-transform infrared (FTIR) and nuclear magnetic resonance (NMR) spectroscopy as well as by gel permeation chromatography (GPC). A method for the preparation of magnetically responsive bionanocomposites (BNCs) was developed consisting of combined dissolution/suspension of the dextran ester and hydrophobized MNPs in an organic solvent followed by homogenization with ultrasonication, casting of the solution, drying and melting of the composite for a defined shaping. This process leads to a uniform distribution of MNPs in BNC as revealed by scanning electron microscope (SEM). Samples of different geometries were exposed to high-frequency alternating magnetic field (AMF). It could be shown that defined remote melting of such biocompatible nanocomposites is possible for the first time. This may lead to a new class of magnetic remote-control systems, which are suitable for controlled release applications or self-healing materials. BNCs containing biocompatible dextran fatty acid ester melting close to human body temperature were prepared and loaded with Rhodamine B (RhB) or green fluorescent protein (GFP) as model drugs to evaluate their potential use as drug delivery system. The release of the model drugs from the magnetic BNC investigated under the influence of a high-frequency AMF (20 kA/m at 400 kHz) showed that on-demand release is realized by applying the external AMF. The BNC possessed a long-term stability (28 d) of the incorporated iron oxide particles after incubation in artificial body fluids. Temperature-dependent mobility investigations of MNP in the molten BNC were carried out by optical microscopy, magnetometry,

***Corresponding author: Thomas Heinze**, Institute of Organic Chemistry and Macromolecular Chemistry, Center of Excellence for Polysaccharide Research, Friedrich Schiller University of Jena, Humboldtstraße 10, D-07743 Jena, Germany, E-mail: thomas.heinze@uni-jena.de
Robert Müller, Leibniz-Institute of Photonic Technology (IPHT), P.O.B. 100239, D-07702 Jena, Germany
Janna Kuchinka, Institute of Organic Chemistry and Macromolecular Chemistry, Center of Excellence for Polysaccharide Research, Friedrich Schiller University of Jena, Humboldtstraße 10, D-07743 Jena, Germany

https://doi.org/10.1515/psr-2019-0122

alternating current (AC) susceptibility, and Mössbauer spectroscopy measurements. Optical microscopy shows a movement of agglomerates and texturing in the micrometer scale, whereas AC susceptometry and Mössbauer spectroscopy investigations reveal that the particles perform diffusive Brownian motion in the liquid polymer melt as separated particles rather than as large agglomerates. Furthermore, a texturing of MNP in the polymer matrix by a static magnetic field gradient was investigated. First results on the preparation of cross-linkable dextran esters are shown. Cross-linking after irradiation of the BNC prevents melting that can be used to influence texturing procedures.

Keywords: drug release, magnetic nanocomposite, thermoplastic dextran

1 Introduction

Magnetic bionanocomposites (BNCs) can open promising opportunities for the design of novel tools for diagnostics and therapies. Today, magnetic BNCs are intensively studied in the field of hyperthermia, [1–3] microfluidic devices, [4, 5], and controlled drug release [6, 7]. Magnetically responsive systems for drug delivery belong to exogenous stimuli-responsive materials, which can react on alternating current (AC) or oscillating magnetic field through two heating mechanisms: (a) hysteresis loss for ferromagnetic particles and/or (b) Néel and Brownian relaxation for superparamagnetic particles and on direct current (DC) magnetic field through targeting [8, 9].

A new approach toward magnetically responsive biomaterials is the use of thermoplastic biopolymers containing magnetic nanoparticles (MNPs). In 2011, an elegant method could be developed for the synthesis of pure dextran fatty acid esters by activation of the carboxylic acids with iminium chloride, which is formed from *N*,*N*-dimethylformamide (DMF) and oxalyl chloride [10]. The bio-based dextran esters obtained are hydrophobic and possess-adjustable melting temperature in the range from room temperature to about 140 °C depending on the detailed structure. The melting temperature could be tailored by the type of substituent introduced, the degree of substitution (DS), and the molecular weight (M_w) of the polymer.

In the frame of own studies, polysaccharide esters were investigated regarding the preparation of magnetic BNC and the properties of the resulting biomaterials. In this chapter, we are going to discuss the synthesis of proper starting thermoplastic polymers dextran esters, the fabrication of the BNC. Moreover, thermoplastic and cross-linkable dextran esters were prepared for the first time and were doped with MNP in order to get barrier forming materials by irradiation with UV light. Studies about the magnetic and thermal behavior were in the center of interest. Moreover, the MNP movement in the molten matrix under a static magnetic field gradient and release properties using model drugs will be highlighted for this new type of magnetic BNC. To get a deeper insight in the new BNC regarding their heating abilities and magnetic

relaxation process, AC susceptometry (ACS) studies were included. ACS is sensitive to the reorientation of magnetic moments in small magnetic fields, realized by Brownian motion or Néel relaxation [11, 12]. Mössbauer spectroscopy was applied as well that represents another versatile technique able to quantify parameters of Néel relaxation. In case of Brownian particle motion, a broadening of absorption lines occurs that allows to determine hydrodynamic radii or the viscosity of the surrounding liquid, respectively [13, 14].

2 Materials and methods

2.1 Materials

Oxalyl chloride, *N,N*-dimethylacetamide (DMAc), and DMF were obtained from Arcos Organics, Geel, Belgium. $FeCl_3 \cdot 6H_2O$ and $FeCl_2 \cdot 4H_2O$, tetrahydrofuran (THF), and oleic acid were obtained from Merck, Darmstadt, Germany. Palmitic acid (PA), myristic acid (MA), and lauric acid (LA) were purchased from Carl Roth GmbH, Karlsruhe, Germany. *N,N′*-carbonyldiimidazole (CDI) was obtained from abcr GmbH, Karlsruhe, Germany. Dimethyl sulfoxide (DMSO) was purchased from Fisher Scientific, Loughborough (U.K). Dextran from *Leuconostoc mesenteroides* ssp. (M_w 6,000, 15,000, and 60,000 g/mol from Sigma Aldrich, Steinheim, Germany) was treated in vacuum at 100 °C for 24 h prior to use. LiCl was supplied by Sigma Aldrich, Steinheim, Germany, and was treated in vacuum for 48 h at 100 °C. 2-[(4-methyl-2-oxo-2*H*-chromen-7-yl)oxy]acetic acid (MUB) was prepared according to [15]. All other reagents were used without further purification.

2.2 Synthesis of dextran ester

2.2.1 Dextran fatty acid ester (2a-l): Dextran fatty acid esters were prepared by activation of fatty acids (LA, MA, and PA) as iminium chlorides following a method described by Liebert et al. [10]. General procedure: Dextran samples of different molar mass (M_w 6,000, 15,000, and 60,000 g/mol) were dissolved in DMAc/LiCl at 100 °C for 1 h under stirring. The fatty acid iminium chloride was prepared by conversion of DMF with oxalyl chloride and subsequent reaction with LA, MA, or PA at – 20 °C for 30 min. Subsequently, the solution of the carboxylic acid iminium chloride was added to the dissolved biopolymer to form the corresponding dextran ester (16 h, 60 °C). After precipitation in isopropanol, the product was dried in vacuum at room temperature for 2 days.

Peracetylation of the dextran esters was carried out to determine the DS by means of ^{1}H NMR spectroscopy according to literature [16]. Details for the esterification and peracetylation of dextran esters are described in Ref. [17].

2.2.2 Dextran-2-[(4-methyl-2-oxo-2*H*-chromen-7-yl)oxy]acetic acid ester (3a,b): Cross-linkable dextran ester was prepared by *in situ* activation of 2-[(4-methyl-2-oxo-2*H*-chromen-7-yl)oxy]acetic acid (MUB) with CDI. To a solution of dextran (M_w 6,000 g/mol, 3.0 g, 18.5 mmol) in DMSO (90 mL), MUB (4.33 g, 18.5 mmol) and CDI (3.0 g, 18.5 mmol) were added and allowed to react at 80 °C for 20 h under stirring. The product was precipitated in 1000 mL ethanol and washed three times. Subsequently, the product was dried under vacuum for 2 days (room temperature) yielding a white solid.

2.2.3 Dextran–MUB fatty acid ester (4a,b): The synthesis of the dextran–MUB fatty acid ester (**4a,b**) was carried out according to the same procedure as described for dextran esters **2a-l** using dextran esters **3a,b** as starting materials.

2.3 Preparation of magnetic nanoparticles

The preparation of MNPs was performed at the Leibniz-Institute of Photonic Technologies (IPHT) and by the group of S. Dutz [18] following a modification of a basic precipitation method described by S. Dutz [19]. Briefly, a solution of 1 M $NaHCO_3$ was slowly added to $FeCl_2/FeCl_3$ solution (Fe^{3+}/Fe^{2+}: 4.2 M/3.3 M) with a rate of 2 mL/min under permanent stirring up to pH 7–7.5, leading to the formation of a brownish precipitate. After that, the solution with the precipitate was boiled for 10 min to form an almost black precipitate. After cooling to room temperature, the suspension was washed with distilled water and dried. Details can be found in [20].

The method described generates bigger MNP than superparamagnetic iron oxide nanoparticles (SPIONs, mean diameter about 15 nm above the superparamagnetic limit) that have larger specific heating power at "high" magnetic field amplitude (Example: 20 kA/m) [21]. The MNPs tend to agglomerate due to the high surface energy and magnetic interaction.

The obtained MNPs were then coated with oleic acid in order to make their surface hydrophobic for a better compatibility within the hydrophobic dextran ester. Oleic acid and concentrated KOH solution were mixed with aqueous suspension of the particles to promote the surfactant in the form of oleate to adhere to the particle surface. The oleate was converted into oleic acid by adding concentrated HNO_3. The mixing steps were done in a ball mill (pulverisette 5, Fritsch, Germany) for 2 h and 150 rpm in order to destroy large agglomerates. The product was washed several times with acetone and hot water alternately. After sedimentation in acetone, supernatant liquid was removed and the substance was dried. Details are described in [22].

2.4 Spectroscopic-, chromatographic- and thermal measurements

Fourier-transform infrared (FTIR) spectra were recorded on a Nicolet Protégé 460 spectrometer with 64 scans and a resolution of 4 cm^{-1} (KBr technique). KBr tablets were dried at 100 °C for 1 h to remove moisture prior to the measurement. Nuclear magnetic resonance (NMR) spectra were acquired on a Bruker AMX 250 spectrometer at room temperature with 16 scans for ^1H NMR, 10,240 scans for ^{13}C NMR measurements, and $^1H/^{13}C$ Heteronuclear Single Quantum Coherence (HSQC) spectra (40 mg sample/mL in $CDCl_3$). The DS values of dextran esters **2a-l** were calculated from ^1H NMR spectra of peracetylated samples (according to Ref. [16]), $DS_{\text{fatty acid}} = 3 - (7 \times I_{\text{H, acetyl}}) / (3 \times I_{\text{H, AGU}})$. The DS values of dextran esters (**3a,b** and **4a,b**) were calculated from elemental analysis (EA), performed with a VARIO EL III CHNS analyzer (Elementar Analysensysteme GmbH Hanau, Germany). The molecular weight was obtained by gel permeation chromatography (GPC, Shimadzu, Japan, calibrated with polystyrene, 370–128,000 g/mol). The samples were dissolved in chloroform/isopropanol/triethylamine (94/2/4) and measured with a flow rate of 1 mL/min at 40 °C. The thermal properties of 10 mg samples were measured by differential scanning calorimetry (DSC, Netzsch DSC 204 F1 Phoenix) in an aluminum pan under nitrogen environment. The heating rate was 10 K/min and cooling rate was 20 K/min. The sample was first cooled to −50 °C and heated up to 200 °C. The heating/cooling cycle was carried out twice. The morphology and distribution of MNP in the polymer matrix were investigated by field emission scanning electron microscopy

(SEM, sputtered with graphite,15 kV, FE-SEM JSM 6300F, JEOL, BSE contrast). One sample with 2.2 wt% MNP was split into two parts by cryogenic break under liquid nitrogen to observe the BNC morphology in the cross-sectional area. UV–Vis spectroscopic investigations were carried out on Lambda 25 UV–Vis Spectrometer (Perkin Elmer, Singapore).

2.5 Magnetic measurements

Static magnetic measurements were carried out with a vibrating sample magnetometer (VSM) Micro-Mag™ 3900 (Princeton Measurements Corp., USA). Magnetization curves M(H) were measured on the unmodified magnetic particles (to get the magnetic phase after preparation), on oleic acid coated particles, and on the BNC for determination of the particle content.

The magnetic alternating current susceptibility (from ACS measurements) of 1 wt% MNP in dextran myristic ester–based biopolymer was measured using a Quantum Design MPMS-5S in the frequency range of 10^2–10^3 Hz at temperatures of 20–120 °C with an applied AC magnetic field amplitude of 4 Oe. Additionally, temperature-dependent magnetization curves of both samples were recorded at 5–390 K with an applied magnetic field of 10 mT following the common zero-field-cooled/field-cooled (ZFC/FC) protocol.

Mössbauer spectra of dextran myristate and palmitate ester–based BNC with 1 wt% of MNP were measured in transmission geometry at temperatures of 20–110 °C using a custom-built setup with a 40 mCi ^{57}Co(Rh) in constant acceleration mode. A BNC sample with thickness of 9 mm was used, corresponding to about 9 mg/cm^2 of nanoparticles. Mössbauer spectra at 4.3 K were measured using a He cryostat containing a superconducting magnet in split-coil geometry providing a uniform magnetic field of up to 5 T. ACS and Mössbauer investigations have been done by research group of Dr. Wende, [23] University of Duisburg-Essen. For details, see their contribution in this book and 35.

2.6 Alternating magnetic field studies

BNCs with different sample geometries, type of polymer, and MNP content were fabricated as described in Section 3.3, in order to study their influence on heating ability by AMF. Disk-shaped BNCs (2 wt% MNP) were made with thickness of 1.4 mm and radius of 8 mm by casting into cylindrical mold. Films of the magnetic BNCs with different MNP concentrations were coated on object glasses by lab applicator into about 30 mm × 20 mm square with thickness of 600 ± 20, 50 ± 3, and 5 ± 1 µm (Table 3). BNC coatings on object glass and disk-shaped samples were placed in the middle of a coil (3 turns and 5.5 cm diameter, water cooled) in air at room temperature and subjected to an AMF amplitude of 20 kA/m and frequency 400 kHz for 5 min. The deviation of the field amplitude in the relevant area inside the coil was measured as smaller than 10 %. The surface temperature of thin film and disk-shaped sample in 1 s interval was monitored by infrared (IR) thermography using a thermal camera (NEC Avio infrared Technology) 20 s before the start of magnetic induction for 5 min and analyzed by InfReC Analyzer NS9500 Standard (frame rate: 1 fps). The results were averaged over three points on the IR thermography. The spatial resolution of the camera combined with the arrangement of the experiment (distance between camera and sample) is about 0.3 mm.

The specific absorption rate (SAR) of the BNC (2 wt% MNP) was determined by measuring the initial heating rate with a fiberoptical sensor (OPTOcon, Dresden, Germany) on a bulk-shaped sample of 0.10 g BNC (granules < 1 mm) in 0.90 g gelatin gel, using the equation $SAR = c \times m_F/m_c \times \Delta T/\Delta t$ with c as the specific sample's heat capacity (value of water), m_c the mass of BNC, m_F the fluid mass, and $\Delta T/\Delta t$ the maximum value of the linear slope of the heating curve after subjecting the sample into an AMF (20 kA/m, 400 KHz) inside of a polystyrene isolation.

3 Results and discussion

3.1 Synthesis and characterization of dextran esters

Esterification of polysaccharides with carboxylic acids is one of the most versatile transformations to create biopolymers with valuable properties [24]. Efficient esterification techniques using special methods and *in situ* procedures for activation of carboxylic acids are a very useful alternative to the conventional reagents (acid chloride or acid anhydride) for the preparation of pure polysaccharide esters [16, 24]. For this purpose, various activating reagents are available, e.g., sulfonic acid chlorides, dialkylcarbodiimide, 1,1′-carbonyldiimadazole (CDI), or activation via iminium chlorides [10, 24].

Studies about esterification of dextran with fatty acids have shown that iminium chlorides of carboxylic acids are in particular efficient [10]. The iminium chlorides of carboxylic acids are formed by the conversion of DMF with chlorinating agents (e.g., phosphoryl chloride, phosphorus trichloride, or oxalyl chloride) and subsequently reaction with the carboxylic acid forming only gaseous by-products. It is a very mild and efficient method for esterification of polysaccharides resulting in pure products [10], which enables biological and medical applications. The polysaccharide dextran, which finds widespread use in medical and pharmaceutical applications, was used for the preparation of thermoplastic bio-based material.

3.1.1 Long-chain fatty acid esters of dextran

Esterification of dextran with long-chain fatty acids is a path to generate thermoplastic products [24]. The synthesis of fatty acid esters was performed by activation of the acids via iminium chlorides using oxalyl chloride as chlorinating agent (Figure 1).

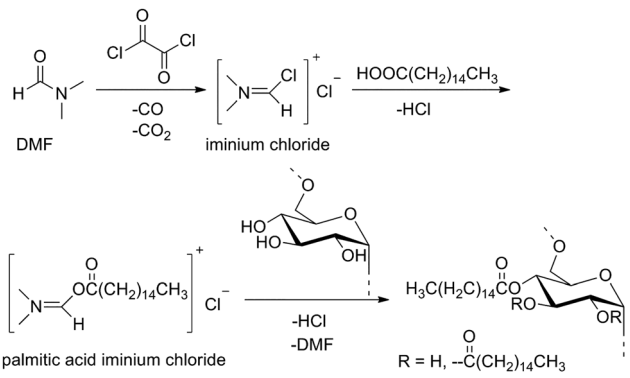

Figure 1: Reaction schema of the conversion of dextran with palmitic acid activated as iminium chloride.

Table 1: Reaction conditions for and results of the esterification of dextran (M_w 6,000 g/mol) with different fatty acids activated as iminium chlorides. (AGU: anhydroglucose unit).

No	Carboxylic acid (C-number)	Molar ratio of AGU:acid	Degree of substitution	Range of melting temperature (°C)
2a	Lauric (12)	1:2	1.06	60–70
2b	Lauric (12)	1:3	1.47	90–98
2c	Lauric (12)	1:5	2.51	30–40
2d	Myristic (14)	1:2	0.98	70–75
2e	Myristic (14)	1:3	1.50	96–105
2f	Myristic (14)	1:5	2.56	40–45
2g	Palmitic (16)	1:2	1.42	100–105
2h	Palmitic (16)	1:3	0.92	130–140
2i	Palmitic (16)	1:5	2.69	42–55
2k[a]	Palmitic (16)	1:2.5	1.59	88–95
2l[b]	Palmitic (16)	1:1.8	1.25	100–105[c]

[a]Prepared with dextran M_w of 15,000 g/mol. [b]Prepared with dextran M_w of 60,000 g/mol. [c]Incomplete melt.

The melting range of the dextran esters can be adjusted by the DS, the type of substituent introduced, and the molecular weight of the polysaccharide. The DS value can be easily controlled by the amount of reagent used. A summary of reaction conditions and results is given in Table 1.

Dextran esters **2a-l** with melting areas in the range of 30 and 140 °C were obtained. Compared to the acids introduced and the M_w of the dextran, the DS value has a significant influence on the melting temperature (Table 1). An increasing DS mostly leads to a lower melting temperature. However, the melting depends on the supramolecular structure of the polymer, i.e., from the interactions of the polymer chains with each other. Thus, the DS and the distribution of the ester moieties may determine the temperature range of the melting, which must not give steady decrease of the temperature with increasing DS. This behavior was also found for the samples with an average DS of about 1.5 that possesses a higher melting temperature compared to samples of lower DS. The structure and the purity of the dextran esters were confirmed with FTIR and NMR spectroscopy.

3.1.2 Cross-linkable dextran ester

In order to generate biomaterial with different magnetic microsegments, dextran was functionalized with a photochemically cross-linkable moiety. Thus, substructures that may have a barrier effect can be created through irradiation with UV light. To produce cross-linkable dextran ester, 2-[(4-methyl-2-oxo-2*H*-chromen-7-yl)oxy]acetic acid (MUB) was chosen as a representative from the well-known coumarin family [25]. Dextran–MUB esters (**3a,b**) were prepared by *in situ* activation of MUB with CDI and conversion with the biopolymer (Figure 2). The dextran–MUB esters (**3a,b**) were further

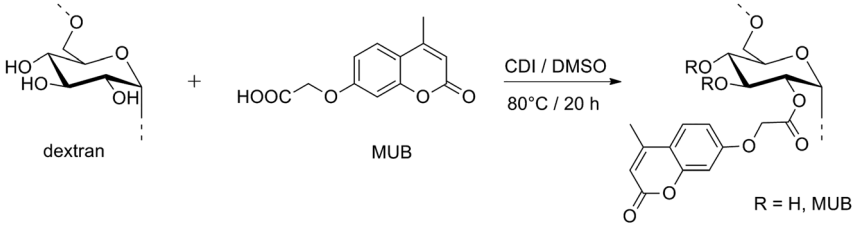

Figure 2: Reaction schema for the preparation of dextran-2-[(4-methyl-2-oxo-2*H*-chromen-7-yl)oxy] acetic acid ester via *in situ* activation of the carboxylic acid with CDI.

esterified with palmitic acid to get thermoplastic biopolymer derivatives (see Section 3.1.1). The DS value can be easily adjusted by the molar ratio both of AGU to MUB and modified AGU to palmitic acid, respectively. A summary of reaction conditions and results is given in Table 2.

Cross-linkable dextran esters **3a** and **3b** possess DS values of 0.19 and 0.62. Thermoplastic and cross-linkable dextran esters were obtained with a range of melting temperature from 58 to 65 °C (**4a**) and from 75 to 80 °C (**4b**). It can be concluded that the temperature of the melting area increased with increasing DS of MUB and decreased with increasing DS of palmitate. The structure and the purity of the different dextran esters (**3a,b** and **4a,b**) were evaluated by means of ^{1}H and ^{13}C NMR spectroscopy.

3.2 Photo-cross-linking

Light-induced cross-linking opens up a possibility for the generation of polymeric networks. It is especially attractive because photo-cross-linking is an ecological and nondestructive process [26]. Moreover, a high level of control over the network formation and cross-linking density can be achieved. Photo-cross-linkable polysaccharides can be generated through functionalization with various photosensitive groups such as cinnamate, anthracene, or coumarin derivatives [27]. These groups are

Table 2: Reaction conditions for and results of the esterification of dextran (M_w 6,000 g/mol) with MUB and of dextran–MUB ester (**3a,b**) with palmitic acid iminium chloride (**4a,b**).

No	Carboxylic acid	Molar ratio (AGU:acid)	Degree of substitution		Range of melting temperature (°C)
			MUB	Palmitate	
3a	MUB	1:0.4	0.19	–	–
3b	MUB	1:1.0	0.62	–	–
4a	Palmitic	1:5.0	0.19	1.92	58–65
4b	Palmitic	1:5.0	0.62	1.66	75–80

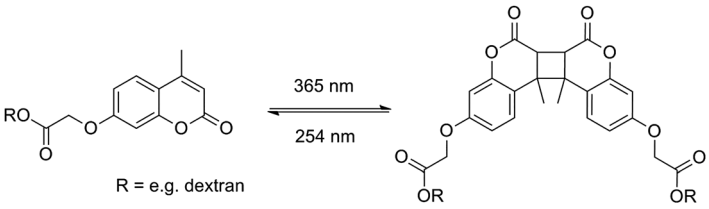

Figure 3: Schematic presentation of the [2π + 2π] cycloaddition of 2-[(4-methyl-2-oxo-2H-chromen-7-yl)oxy]acetic acid derivative.

able to form covalent bonds under controlled UV-light irradiation via photodimerization, which may be reversible depending on the wavelength of the light. Coumarin derivatives, e.g., undergo a [2π + 2π] cycloaddition forming a cyclobutane during irradiation at wavelength above 300 nm, whereas cleavage occurs at 254 nm (Figure 3)[27].

The photochemical response of dextran esters **4a** and **4b** was studied in solution by means of UV–Vis spectroscopy under irradiation with light of a wavelength of 365 nm (Figure 4). Upon irradiation, the absorption at 316 nm decreases indicating the formation of the MUB dimer via [2π + 2π] cycloaddition. After 180 min, a degree of dimerization of 50 % for **4a** and around 70 % for **4b** was achieved, concluding that the material with a higher DS of cross-linkable groups shows better cross-linking behavior. Furthermore, the absorbance increases with increasing DS of MUB because of the relative higher content of coumarin moieties.

Photo-cross-linking experiments with films of dextran esters **4a** and **4b**, prepared with a lab applicator, were carried out. The films were irradiated for 3 h with light of a wavelength λ = 365 nm to investigate the cross-linking ability in the solid state. The films obtained show changes of properties, including solubility and melting behavior. Irradiated films of dextran ester **4b** do not melt anymore, whereas films prepared from **4a** are still partially meltable. It can be concluded that a DS of MUB of 0.19 is not sufficient to obtain a complete cross-linking of the material.

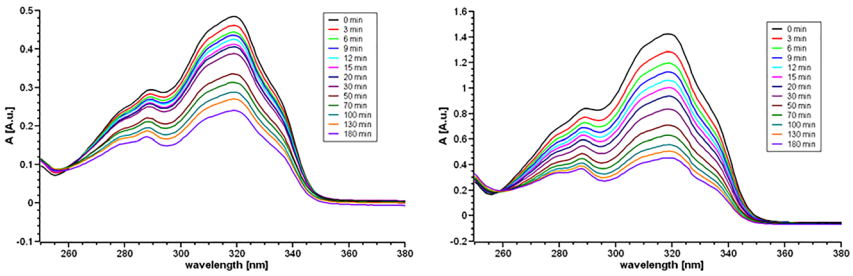

Figure 4: UV–Vis spectra of the photodimerization of **4a** (left) and **4b** (right) dissolved in $CHCl_3$ after different irradiation times.

3.3 Preparation and analysis of magnetic bionanocomposite (BNC)

The dextran ester and the MNPs were analyzed by different methods including FTIR spectroscopy, DSC, thermal gravimetric analysis (TGA), viscosimetry, dilatometry, hot table microscope (for polymers), and dynamic light scattering (DLS) and vibrating sample magnetometry (for MNP).

Modification of iron oxide nanoparticle with carboxylic acid results from the interactions between the carboxylic/carboxylate moieties and the surface metal ion [28]. Uncoated MNP shows a coercivity H_C of 3.1 kA/m and a saturation magnetization M_S of 74.8 Am^2/kg, oleic acid–coated MNP a decreased H_C of 2.5 kA/m and M_S of 68.8 Am^2/kg. From M_S measurements the content of oleic acid was calculated. It is in the range of 8 wt%. Dextran myristate (**2f**) and dextran palmitate (**2i**), showing melting points in the region suitable for applications in the biological field, were chosen for fabrication of magnetic hybrid material and were applied for the following experiments.

In the frame of these studies, three different approaches were investigated for fabrication of magnetic BNCs, namely mixing of the polymer and the MNP, followed by melt extrusion, dissolution/suspension of polymer, and film formation on glass by spin coating [17]. However, only dissolution/suspension combined with solution casting and subsequent coating with lab applicator on glass after melting was used to prepare BNC for the studies, bulk samples and layers, respectively, for all types of dextran ester. In detail, magnetic BNCs with MNP concentrations between 0.05 and 2.2 wt% were obtained by following steps: dissolution of the dextran ester (2.0 g including MNP) and suspending hydrophobized MNPs in the organic solvent tetrahydrofuran (THF) followed by homogenization with ultrasonication (Elma Transsonic 460/H) for 20 min and evaporation of the solvent by drying of thin layers under air flow. The material was collected in the form of granulates, dried in vacuum to remove residual THF, and shaped in the molten state. The BNCs were coated on object glasses into 20×30 mm^2 square with thickness of 5, 50, and 600 μm or casted to disks of up to 1.4 mm thickness. The used preparation method gives a uniform dispersion of MNP in the polymer matrix. The parameters of the different samples can be seen in Table 3.

The spatial distribution and morphology of MNP in the polymer were studied by SEM and optical microscope (Figure 5). In a sample containing 2.2 wt% of MNP, the MNP and small agglomerates in range between 100 nm and 1 μm are uniformly distributed in the polymer matrix (**2i**, Figure 5). The SEM picture shows that the particles are also well distributed. The evenly distributed particles could also be seen in the cross-sectional direction of a sliced sample (Figure 5, right). Less aggregates are formed in samples with a smaller MNP content [17]. The MNPs are interlocked in the polymer matrix.

Rheological measurements on dextran palmitate in a magnetic field of 100 kA/m have been performed by D. Borinx [30]. Control of the gradient-free sample temperature

Table 3: Summary of composition and geometry of magnetic BNC fabricated by solution casting and their maximal heating response by IR thermography on alternating magnetic field (AMF) heating.

No	Composition	Sample geometry	Thickness (µm)	Maximal ΔT (°C)[a]	Heating rate (mK/s)[b]
C1	**2i** + 2 wt% MNP	Coating film	600 ± 20	25	114
C2	**2i** + 2 wt% MNP	Coating film	50 ± 3	7	32
C3	**2i** + 2 wt% MNP	Coating film	5 ± 1	1	5
C4	**2i** + 1 wt% MNP	Coating film	50 ± 3	4	14
C5	**2i** + 0.3 wt% MNP	Coating film	50 ± 3	1	4
C6	**2i** + 0.05 wt% MNP	Coating film	50 ± 3	0	0
C7	**2i** (control sample)	Coating film	50 ± 3	0	0
C8	**2i** + 2 wt% MNP	Disk sample (r = 8 mm)	1400 ± 50	38	136
C9	**2i** + 2 wt% MNP	Disk sample (r = 8 mm)	1400 ± 50	33	138
C10	0.1 g **2i** + 2 wt% MNP in 0.9 g gelatin	Granules (< 1 µm)	–	30	88

[a]Subtracted by control sample. [b]Heating rate (maximum temperature divided by the time, measuring frequency: 1 Hz).

was ensured with a Peltier hood. After the tempering procedure, an examined sample has been pre-sheared at a shear rate of 100 1/s at least during 120 s and the external magnetic field was applied using the same shearing conditions. The measurements show only a weak effect of the magnetic field of about 0.8 % viscosity increase at 60 °C and 2.8 % increase at 100 °C, respectively, that is a further indication of the weak magnetic interaction between the particles. The magnetic effect is reversible.

A further indication of the spatially averaged, predominant particle interaction depending on the particle distance can be obtained from the Henkel plot [31] that can

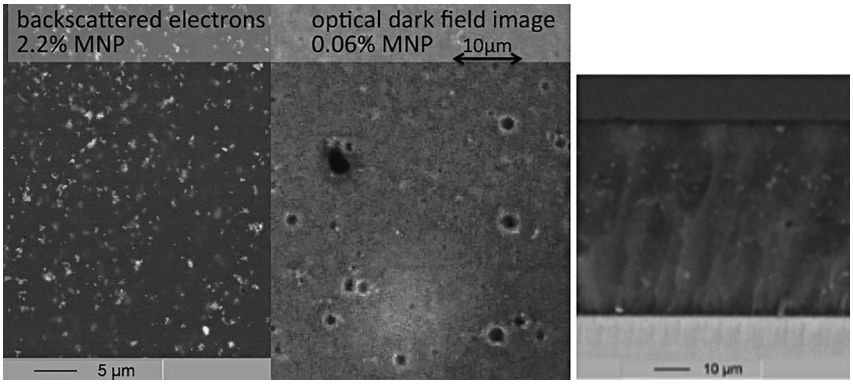

Figure 5: SEM (left) and optical image (center) of MNP in dextran ester 2i and SEM image (right) of cross section of the 2.2 w.t% MNP layer (fracture surface). © [2015] IEEE. Reprinted, from [45].

be derived from the initial and the demagnetization remanence curves. Both remanence curves are related via the relation of Wohlfarth [32] in the absence of interaction (straight line in Figure 7). In Figure 7, only weak particle interaction in samples with dispersed particles is shown, almost independent from the MNP concentration. In order to show the effect of a particle agglomeration in the Henkel plot, the polymer matrix of a composite sample with 2.2 wt% of MNP was dissolved and the sample was measured in liquid state, i.e., after agglomeration.

Magnetic measurements by VSM were carried out to compare magnetic particle–particle interaction that depends on the mean particle distance. Increasing hysteresis parameters (H_c, remanence ratio M_r/M_s) with decreasing particle content were found that suggests a decreasing magnetic interaction, i.e., a better separation of particles on microscopic scale (Figure 6) [29]. The particle content was calculated from magnetization values.

DSC measurements were carried out to evaluate if the embedment of particles modifies the thermal behavior of the dextran esters. The first heating curve of dextran palmitic ester and BNC obtained with this sample (1 and 2 wt% of MNP) is shown in

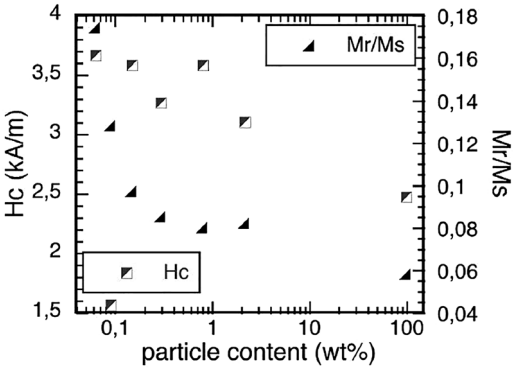

Figure 6: Hysteresis parameters vs. MNP concentration. © [2015] IEEE. Reprinted, from [45].

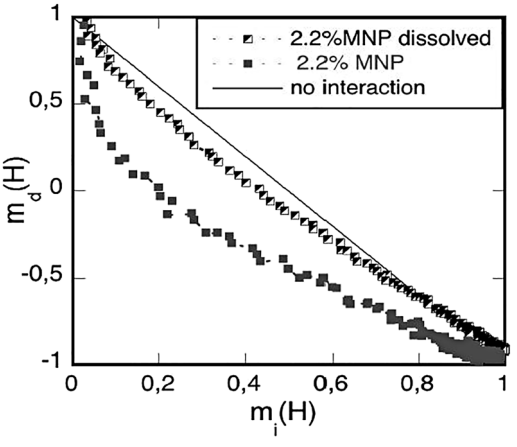

Figure 7: Henkel plot (magnetic interaction) of different MNP arrangement. © [2015] IEEE. Reprinted, from [45].

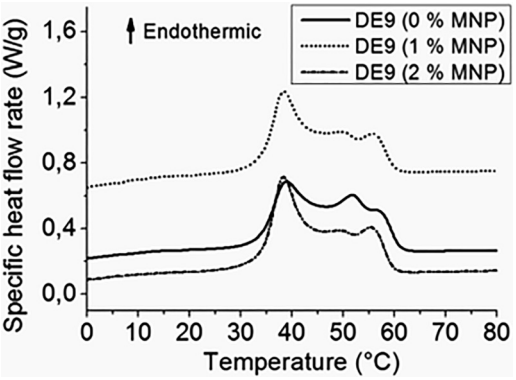

Figure 8: Thermal behavior of dextran palmitic ester and BNC characterized by DSC, solid line, 2i; point, 2i with 1 w.t% MNP; dash-point, 2i with 2 w.t% MNP. Reprinted from 17 Copyright (2015) American Chemical Society.

Figure 8. An endothermic peak is found at 39 °C for dextran palmitic ester and two additional peaks at 50 °C and 56 °C that is the same temperature range observed optically as melting region. Detailed assignment of these peaks is not yet possible. Nevertheless, the DSC measurements of the BNC of **2i** show the same signals with comparable intensities, which means the presence of the MNP does not affect the thermal behavior of dextran ester.

3.4 Alternating magnetic field heating experiments

The internal melting behavior of the BNC depends on type of polymer, MNP content, and geometry of the sample. Heating experiments in an AMF based on magnetic losses of the MNP in the composite material have been done to find temperature limits using certain geometrical arrangements of the samples in comparison to melting temperatures of the dextran ester and the specific absorption rate of the BNC. Such experiments are precondition for further thermal-driven drug release experiments.

The heating response of magnetic BNC on glass with different geometries (thickness 5, 50, and 600 μm) and MNP content to AMF was studied in detail (Table 3) [17]. BNC films on glass were placed in the middle of a coil at room temperature and exposed to an AMF of 20 kA/m and frequency of 400 kHz for 5 min. The surface temperature of the thin films was monitored by IR thermography using a thermal camera 20 s before and 5 min after the magnetic induction. Details on these measurements are given in [17]. A typically uniform heating response of the sample (**C2**) on application of AMF is generated due to the good dispersion of MNP in the BNC layer (Figure 9, left). AMF for longer times increases the surface temperature, correspondingly. The heating response is strongly dependent on the thickness of the layer [17] because of heat dissipation through conduction to the glass substrate and convection to air depending on the ratio of the surface area to volume (Figure 9, right). The maximal increase in temperature after 5 min and the corresponding heating rates measured on the coating films without

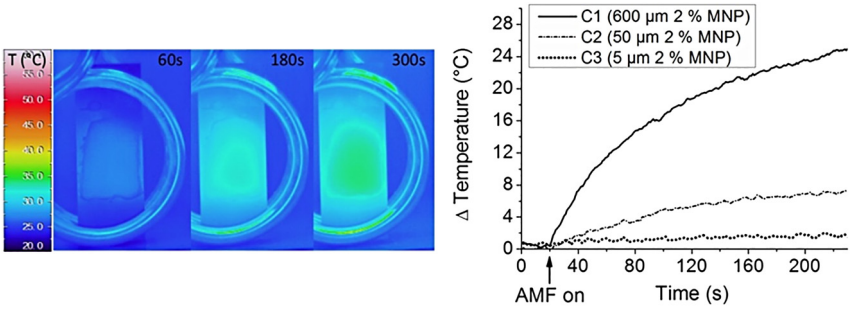

Figure 9: IR thermography of a film prepared from sample **C2** after 60, 180, and 300 s in AMF (left). The graph (right) shows the surface temperature (subtracted by control sample **C7**) of the BNC films **C1–C3** subjected to continuous AMF. Reprinted from 17 Copyright (2015) American Chemical Society.

MNP are listed in Table 3. When the MNP loading is below 1 wt% (**C5, C6**), there is no significant heating response for samples with thickness of 50 µm.

Disk-like shaped samples with thickness of 1.4 mm and radius of 8 mm were prepared by casting into a cylindrical mold to diminish heat dissipation compared to the films on glass and were placed on a polystyrene holder in the middle of coil. After 2–3 min, such disk-type samples were heated above the melting temperature (**C8**: 50 °C, **C9**: 45 °C) of the dextran ester, i.e., these samples have a much better heating rate than the films (Table 3). After switching off the AMF, the BNCs were quickly cooled in air under the melting temperature and solidified within 2 min (Figure 10, right) that confirms that the material is in principle very well suitable for remote melting, e.g., in controlled release applications.

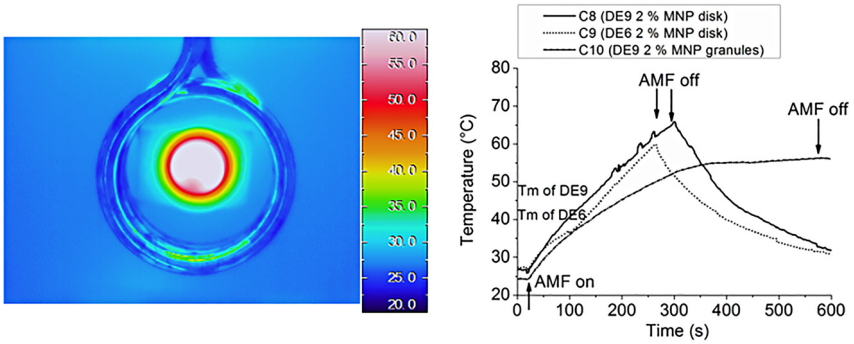

Figure 10: IR thermography of sample **C8** after 240 s in an AMF (left); surface temperature of BNC disk of samples **C8** and **C9** in comparison to sample **C10** subjected to continuous AMF (right). Reprinted from 17 Copyright (2015) American Chemical Society.

Further heating experiments were performed in an arrangement more comparable to a medical application, like drug release, on small bulk-shaped samples in water or in gelatin as biological model system. Measuring the temperature of the surrounding water at known mass ration sample/water, the SAR of the sample material can be calculated from the initial heating rate. Here the temperature was measured with a fiber-optical sensor (OPTOcon, Dresden, Germany).

The SAR of the BNC **C10** (10 wt% in gelatin, 2.2 wt% MNP) was determined as 6.3 W/g (Figure 10, right), which was subjected to AMF (20 kA/m, 400 kHz). A specific heat capacity of 1.5 kJ/kg·K was assumed. A plateau in the heating curve at 55 °C was found and lasted for about 80 s. The temperature went to 54 °C until the field was turned off. The heating rate is smaller compared to disk samples, because the heat was absorbed by water. Nevertheless, even in this setup melting of the BNC was readily achieved.

3.5 Texturing experiments

In a molten polymer matrix (dextran palmitate **2i** with different content of MNPs, by AMF or external heating), the MNP can be moved inside the matrix by a magnetic field gradient. Our experiments revealed such a movement by application of an external static magnetic field (NdFeB magnet, field gradient about 15–20 T/m). In samples with a low concentration of particles (< 0.2 %), the movement of single particles in the matrix is microscopically observable. Particle velocities of up to 0.25 mm/s were observed at sample temperatures of about 100 °C leading to a viscosity of about 1 Pa s. This movement can be influenced by a superposition with convection or viscosity deviations by a thermal gradient in the case of a nonuniform heating source. In samples with a higher MNP concentration (> 0.5 %), we observed a "magnetic texturing" of the BNC under a static field, which alters the SAR after switching off the DC field (Figure 11).

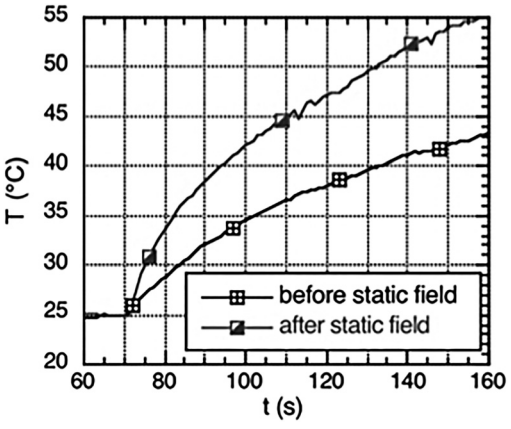

Figure 11: Maximum temperature of the BNC in an AMF before and after texturing in a static magnetic field. Texturing axis was perpendicular to the BNC layer = parallel to AMF. © [2015] IEEE. Reprinted, from [45].

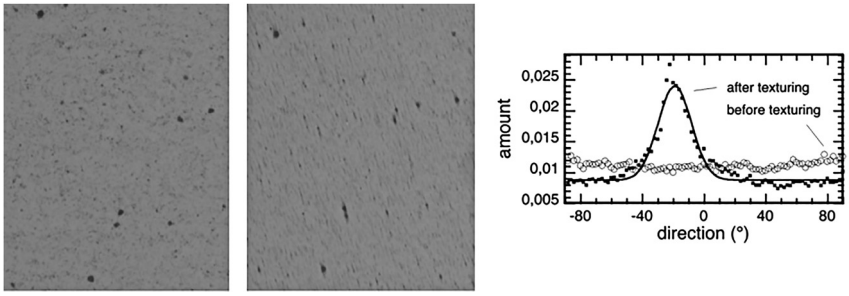

Figure 12: Proof of particle texturing in a static magnetic field under external heating at 80 °C/5 min: Optical image before (left) and after (right) texturing and corresponding pixel analysis (0° = y-direction). © [2015] IEEE. Reprinted, from [45].

The structural reason for that (orientation of MNP and agglomerates or increase of the local MNP concentration) is not investigated yet.

In addition to optical micrographs, a "magnetic texturing" can be seen by pixel analysis (in-plane direction of pixel structures, [33] for details, see [34]) in Figure 12. The pixel analysis reveals a distribution of the area of "similar pixels" (not of particles). The texturing axis corresponds roughly with the direction of the field gradient. Before texturing, the image reveals no preferred direction of pixel structures, i.e., there is no particle texturing caused by formation of the BNC films. The dependence of the quasi-static hysteresis losses (area of the VSM magnetization loop) on the direction concerning the texture axis was investigated on a textured sample of about 10 mm^3 at a maximum field strength (20 kA/m) similar to the AMF amplitude (Figure 13). The losses measured perpendicular to the texturing axis are higher by a factor of 1.7 compared to these measured parallel to the texturing axis (losses per magnetization cycle: $2.0 \cdot 10^{-8}$ J vs. $1.2 \cdot 10^{-8}$ J). Further minor loop parameters are given in [35].

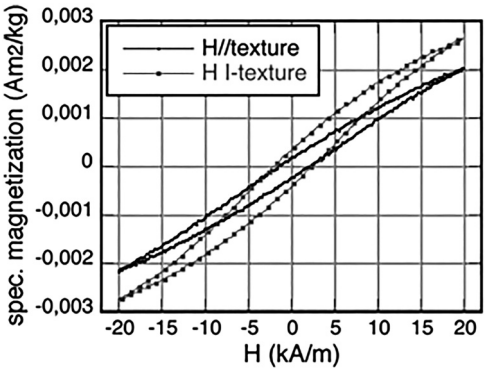

Figure 13: Minor magnetization curves measured parallel and perpendicular to the texturing axis. © [2015] IEEE. Reprinted, from [45].

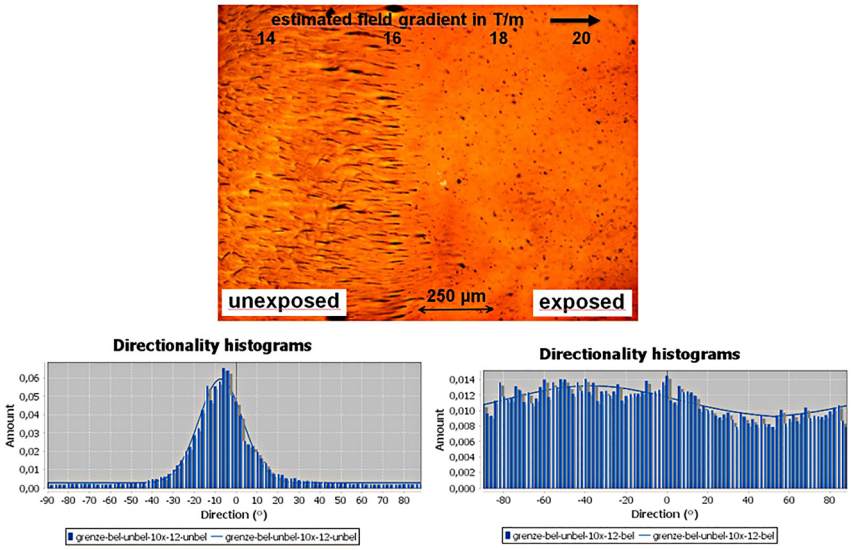

Figure 14: Particle texturing in a static magnetic field under external heating at 110 °C/5 min: optical image without (left side) and with previous irradiation at 365 nm (right side) after texturing and corresponding pixel analysis (0° = y-direction).

Furthermore, texturing experiments of particles in cross-linkable biopolymer (dextran ester **4b** with 2 wt% MNP, film thickness 250 µm, external heating (110 °C/5 min)) by a static magnetic field were performed. The BNC was coated on object glasses and a defined sector was irradiated with UV light. A movement of MNP could be only observed in the area of unexposed BNC (Figure 14). Pixel analysis (in-plane direction of pixel structures) [33, 34] of the corresponding areas of the optical image and magnetic measurements confirm the texturing.

3.6 Magnetometry and AC susceptometry experiments

The general magnetic relaxation behavior of dextran myristate **2f** and palmitate **2i** ester with MNP was investigated in [35] by recording ZFC/FC magnetization curves between 5 and 390 K using an applied magnetic field of 10 mT. Since the irreversibility temperature at which both magnetization curves coincide is not reached, one can conclude that in both samples there is at least a minor fraction of larger multicore particles showing sufficiently slow Brownian relaxation to be considered as magnetically blocked on the magnetometry time scale.

The average hydrodynamic diameter of the MNP (or agglomerates) moving in the liquid polymer melt can be determined by measurements of the magnetic AC susceptibility [36]. The imaginary component χ'' of the magnetic susceptibility is given by

$\chi'' = \chi' \omega\tau/(1+(\omega\tau)^2)$, $\tau = \pi\eta V_h/k_B T$ (ω: angular frequency, τ: relaxation time, η: dynamic viscosity, $k_B T$: thermal energy, χ': static susceptibility). Effects of the particle diameter distribution, resulting in a shift of the average Brownian relaxation time and a broadened peak in χ'', were considered as described in [35]. The influence of the oleic acid coating with about 1–2 nm in thickness can be neglected compared to the total particle size. The thickness of the oleic acid coating of ferrite particles coated by a similar procedure was found by SANS investigations [37].

ACS shows measurements of the imaginary part χ'' of the magnetic susceptibility of 1 wt% MNPs in the dextran myristate–based sample at different temperatures. For temperatures below the melting region, χ'' is found to be relatively constant that is presumably caused by slow Néel relaxation processes with a broad distribution of relaxation times and is in agreement with the absence of a distinct Néel relaxation peak in ZFC magnetization curves. Whereas far above the melting region, a broad peak at the low frequency regime can be seen, moving toward higher frequencies with increasing temperature [35].

Assuming a polymer melt viscosity of about 0.5 Pa s at 393 K, an average particle diameter of approx. 64 nm and a width of the log normal size distribution of 36 nm could be calculated [35]. Taking into account the size of the multicore particles of about 30–80 nm found by SEM, this indicates that Brownian motion in the liquid polymer melt is dominated by the movement of separate particles rather than large agglomerates. However, high relaxation times of large agglomerates in a high viscous melt might be outside of the accessible measurement range using ACS.

3.7 Mössbauer spectroscopy

Mössbauer investigations on magnetic BNC were carried out by the group of Dr. H. Wende (University of Duisburg-Essen) [23]. In the present paper only a short summary of the results is given. Details can be found in [35].

Mössbauer spectra of the dextran myristate **2f** BNC were measured at different temperatures with and without an applied magnetic field of 5 T, respectively. Figure 15 shows an example of a measurement (temperature: 4.3 K, magnetic field: 0T). Further spectra are available in [35]. The spectra display a magnetically ordered sextet structure reproducible by three sextet subspectra, [38] Fe^{3+} and Fe^{2+} on octahedral sites and Fe^{3+} on tetrahedral sites, a mixture of magnetite and maghemite within the particles, and an insignificant fraction of paramagnetic material. Furthermore, the relative line intensities indicate a low degree of spin canting that may suggest a well-ordered magnetic structure of the studied iron-oxide particles. The influence of Néel relaxation taking into account the lognormal particle diameter distribution [39] could be seen by measurements at different temperatures [35]. Details of reproducing the spectra can be found in [35]. Considering limitations in the time constant of Mössbauer spectroscopy and of magnetic exchange and interaction effects, only a rough approximation of the

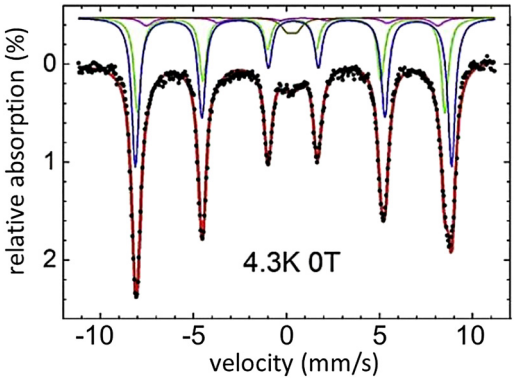

Figure 15: Mössbauer spectrum of dextran myristate–based sample measured at 4.3 K without an applied magnetic field along γ-ray propagation direction, showing a typical sextet structure and the deconvolution of the spectrum.

particles' anisotropy was possible. An effective anisotropy constant of about 18 kJm^{-3} was estimated assuming an average size of about 15 nm of the crystallites.

Effects of particle motion can also be observed by Mössbauer spectroscopy, measuring the broadening of the absorption lines caused by the diffusive translational motion of the particles within the polymer melts above the melting temperature. The line broadening is independent of the Néel relaxation process. Details on the analysis of the data are given in [35]. A first considerable line broadening of dextran myristate and palmitate BNC can be observed in the melting region of the samples. A slow, exponential increase in line width caused by the decrease in polymer melt viscosity at higher temperatures indicates an enhanced particle mobility as it was illustrated by AC susceptometry data.

3.8 Cell experiments/biocompatibility studies

For a possible biomedical application of the dextran ester BNC cell experiments for biocompatibility studies are necessary and were carried out by the group of J. Clement (University Hospital, Jena) [40]. Human brain microvascular endothelial cells (HBMECs) representing the human blood–brain barrier were used for testing biocompatibility of the dextran ester and their coating *in vitro*. The cells were seeded on the dextran ester–coated coverslips within 24 well plates and cultured for 48 h. For microscopic investigation of cell viability, adherent cells were washed with phosphate buffered saline, fixed in neutral buffered formalin, and subsequently, the cell membrane was permeabilized in 0.1 % Triton-X 100 (Sigma-Aldrich Chemie, Steinheim, Germany). For visualization and microscopic characterization, both F-actin (a protein that forms microfilaments in the cytoskeleton) and nuclei of the cells were stained simultaneously. Fluorescence was analyzed using the confocal laser scanning microscope LSM 510 META (Carl Zeiss Microscopy GmbH, Jena, Germany). Details are given in [17].

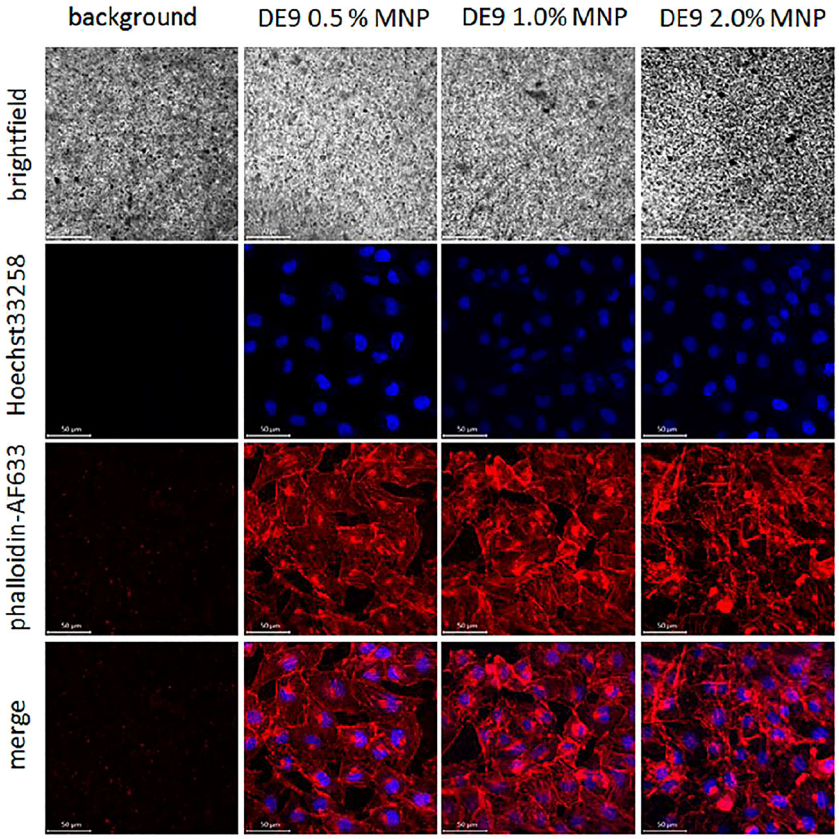

Figure 16: HBMC were seeded on dextran ester **2i** containing MNP concentrations of 0.5, 1.0, and 2.0 % immobilized on glass coverslips. Upon fixation and permeabilization, nuclei and F-actin were stained with Hoechst33258 (blue) and Alexa Fluor phalloidin 633 (red), respectively. Stained samples were analyzed by confocal laser scanning microscopy with 400-fold magnification. Scale bars indicate 50 µm. Reprinted from 17 Copyright (2015) American Chemical Society.

In the experiment, HBMECs were covered by increasing concentrations of MNP embedded within dextran ester **2i**. The cells attach to the dextran ester surface in a well-distributed manner and show a regular cellular growth compared to control cells on glass coverslips without any composite coating (Figure 16). The staining of F-actin indicates that the presence of dextran ester with particle concentrations between 0.5 and 2.0 % does not influence the cell morphology and cell–cell contacts do not appear disrupted. Additionally, a recovery of a numbers of cells from the dextran-coated surface was observed. That means these results confirm a biocompatible nature of this BNC containing up to 2.0 % magnetic particles.

Furthermore, investigations on the biodegradation of the BNC in artificial body fluids (simulated body fluid, SBF; pH 7.4) and artificial lysosomal fluid (ALF, pH 4.5)

that may influence the applicability of BNC in medicine were carried out by D. Fischer [41]. SBF simulates a neutral body environment (pH 7.4) that can be found in the blood stream, the extracellular matrix, or in the cytoplasm. ALF was used to simulate the degradation of potentially released iron oxide particles from the BNC and to assess the shielding effect of the dextran fatty acid ester in acidic environments. The iron release from the incorporated MNPs was used as a measure for the stability of the material. The measurements are described in [42]. Only 0.31 % (dextran palmitate) or 0.19 % (dextran myristate) of the total iron content was released during storage in SBF indicating the stability of the MNP in the BNC, whereas in ALF higher cumulative amount of 5.4 % (dextran palmitate) or 2.17 % (dextran myristate) was mobilized after 28 d at 37 °C, which is in accordance with pH-dependent results of Gutiérrez et al. [43]. It might be that the hydrophobicity of the dextran esters prevents degradation by limiting the penetration of the aqueous simulation media into deeper regions of the BNC and therefore only superficial areas degraded. This indicates a sufficient stability of the BNC that could be used as remote-controlled drug delivery systems or for the induction of hyperthermia [44] over a long period. The dextran fatty acid esters are able to protect the incorporated MNP from degradation even at acidic conditions (ALF). There were no significant differences regarding the stability of the BNC between the two investigated polymers dextran myristic ester and dextran palmitic ester.

4 Conclusion

It is shown that thermoplastic magnetic BNC can be prepared from dextran fatty acid ester and MNPs with melting temperatures slightly above human body temperature and beyond (>100 °C). The heating response of BNC to the application of high-frequency AMF depends on MNP content and geometry of the sample. With an optimal content of MNP between 1 and 2 wt% and a thickness of at least 50 µm, heating above the melting temperature is possible. In the molten state of the BNC, a texturing of MNP is possible by means of a static magnetic field that improves the heating ability of the material. AC susceptometry reveals that the MNPs perform diffusive Brownian motion in the liquid polymer melt as separated particles rather than large agglomerates. Mössbauer spectroscopy confirms this result in respect to a clear increase of particle mobility at temperatures of 50–110 °C and further indicates a well-ordered magnetic structure within the particles. Furthermore, meltable dextran ester can be functionalized with a photochemically cross-linkable moiety. Irradiation of cross-linkable BNC with UV light leads to changed properties, including solubility and melting behavior.

Acknowledgment: The financial support of the German Science Foundation DFG, priority program SPP 1681, contracts HE2054/14-1, HE2054/14-2, HE2054/22-1, and MU2382/4-1, MU2382/4-2, MU2382/5-1 is gratefully acknowledged.The authors are very thankful to former coworkers in the project: M. Zhou, Dr. N. Kuhl, and A. Dellith.The

authors thank the colleagues of the priority program SPP 1681 for useful discussions and especially Dr. D. Borin/Prof. Dr. S. Odenbach (Technical University of Dresden) for rheological measurements, Prof. Dr. S. Dutz and coworkers (Technical University of Ilmenau) for the preparation of the magnetic nanoparticles, Dr. J. Clement (University Hospital, Jena) for cell experiments for biocompatibility studies, Prof. Dr. D. Fischer and coworkers (Friedrich-Schiller University of Jena, no SPP member) for investigations on the biodegradation of the bionanocomposites in artificial body fluids, and Dr. J. Landers/Prof. Dr. H. Wende and coworkers (University of Duisburg-Essen) for ACS and Mössbauer investigations.

Author contribution: All the authors have accepted responsibility for the entire content of this submitted manuscript and approved submission.

Research funding: Deutsche Forschungsgemeinschaft Award Numbers :HE2054/14-1HE2054/14-2HE2054/22-1MU2382/4-1MU2382/4-2MU2382/5-1.

Conflict of interest statement: The authors declare no conflicts of interest regarding this article.

References

1. Gupta AK, Gupta M. Synthesis and surface engineering of iron oxide nanoparticles for biomedical applications. Biomaterials 2005;26:3995–4021.
2. Sadhukha T, Wiedmann TS, Panyam J. Inhalable magnetic nanoparticles for targeted hyperthermia in lung cancer therapy. Biomaterials 2013;34:5163–71.
3. Sadhukha T, Wiedmann TS, Panyam J. Enhancing therapeutic efficacy through designed aggregation of nanoparticles. Biomaterials 2014;35:7860–9.
4. Satarkar NS, Zhang W, Eitel RE, Hilt JZ. Magnetic hydrogel nanocomposites as remote controlled microfluidic valves. Lab Chip 2009;9:1773–9.
5. Wilson SA, Jourdain RP, Zhang Q, Dorey RA, Bowen CR, Willander M, et al. New materials for micro-scale sensors and actuators: an engineering review. Mater Sci Eng R Rep 2007;56:1–129.
6. Satarkar NS, Biswal D, Hilt JZ. Hydrogel nanocomposites: a review of applications as remote controlled biomaterials. Soft Matter 2010;6:2364–71.
7. Satarkar NS, Hilt JZ. Magnetic hydrogel nanocomposites for remote controlled pulsatile drug release. J Contr Release 2008;130:246–51.
8. Mura S, Nicolas J, Couvreur P. Stimuli-responsive nanocarriers for drug delivery. Nat Mater 2013; 12:991–1003.
9. Qiu Y, Park K. Environment-sensitive hydrogels for drug delivery. Adv Drug Deliv Rev 2001;53:321–39.
10. Liebert T, Wotschadlo J, Laudeley P, Heinze T. Meltable dextran esters as biocompatible and functional coating materials. Biomacromolecules 2011;12:3107–13.
11. Chung S-H, Hoffmann A, Guslienko K, Bader SD, Liu C, Kay B, et al. Biological sensing with magnetic nanoparticles using brownian relaxation. J Appl Phys 2005;97:10R101.
12. Zeisberger M, Dutz S, Müller R, Hergt R, Matoussevitch N, Bönnemann H. Metallic cobalt nanoparticles for heating applications. J Magn Magn Mater 2007;311:224–7.
13. Keller H, Kündig W. Mössbauer studies of brownian motion. Solid State Commun 1975;16:253–6.
14. Landers J, Salamon S, Remmer H, Ludwig F, Wende H. Simultaneous study of brownian and Néel relaxation phenomena in ferrofluids by mössbauer spectroscopy. Nano Lett 2016;16:1150–5.

15. Chimichi S, Boccalini M, Cosimelli B. A new convenient route to 2-oxoethoxycoumarins: key intermediates in the synthesis of natural products. Tetrahedron 2002;58:4851–8.
16. Liebert TF, Heinze T. Tailored cellulose esters: synthesis and structure determination. Biomacromolecules 2005;6:333–40.
17. Zhou M, Liebert T, Müller R, Dellith A, Gräfe C, Clement JH, et al. Magnetic biocomposites for remote melting. Biomacromolecules 2015;16:2308–15.
18. Preparation of magnetic nanoparticles was carried out by Dr. S. Dutz. Institute of Biomedical Engineering and Informatics. Germany: Technical University of Ilmenau. 98693.
19. Dutz S, Andrä W, Hergt R, Müller R, Oestreich C, Schmidt C, et al. Influence of dextran coating on the magnetic behaviour of iron oxide nanoparticles. J Magn Magn Mater 2007;311:51–4.
20. Müller R, Dutz S, Habisreuther T, Zeisberger M. Investigations on magnetic particles prepared by cyclic growth. J Magn Magn Mater 2011;323:1223–7.
21. Müller R, Dutz S, Neeb A, Cato ACB, Zeisberger M. Magnetic heating effect of nanoparticles with different sizes and size distributions. J Magn Magn Mater 2013;328:80–5.
22. Müller R, Hiergeist R, Steinmetz H, Ayoub N, Fujisaki M, Schüppel W. Barium hexaferrite ferrofluids–preparation and physical properties. J Magn Magn Mater 1999;201:34–7.
23. Mössbauer investigations were carried out by the group of Dr. H. Wende. Faculty of Physics and Center for Nanointegration Duisburg-Essen. Germany: University of Duisburg-Essen. 47057.
24. Heinze T, Liebert T, Koschella A. Esterification of Polysaccharides. Berlin, Heidelberg, Germany: Springer Science & Business Media; 2006.
25. Wondraczek H, Heinze T. Efficient synthesis and characterization of new photoactive dextran esters showing nanosphere formation. Macromol Biosci 2008;8:606–14.
26. Defize T, Thomassin J-M, Ottevaere H, Malherbe C, Eppe G, Jellali R, et al. Photo-cross-linkable coumarin-based poly (ε-Caprolactone) for light-controlled design and reconfiguration of shape-memory polymer networks. Macromolecules 2018;52:444–56.
27. Trenor SR, Shultz AR, Love BJ, Long TE. Coumarins in polymers: from light harvesting to photo-cross-linkable tissue scaffolds. Chem Rev 2004;104:3059–78.
28. Soler MAG, Alcantara GB, Soares FQ, Viali WR, Sartoratto PPC, Fernandez JRL, et al. Study of molecular surface coating on the stability of maghemite nanoparticles. Surf Sci 2007;601: 3921–5.
29. Dutz S, Hergt R. The role of interactions in systems of single domain ferrimagnetic iron oxide nanoparticles. J Nano Electronic Phy; 2012;4:20101–7.
30. Rheological measurements were carried out by Dr. D. Borin. Institute of Fluid Mechanics, Germany. Technical University of Dresden. 01062.
31. Henkel O. Remanenzverhalten und wechselwirkungen in hartmagnetischen teilchenkollektiven. Phys Status Solidi 1964;7:919–29.
32. Wohlfarth EP. Relations between different modes of acquisition of the remanent magnetization of ferromagnetic particles. J Appl Phys 1958;29:595–6.
33. Available at: https://imagej.net/Fiji.
34. Available at: https://imagej.net/Directionality.
35. Müller R, Zhou M, Liebert T, Landers J, Salamon S, Webers S, et al. Mobility investigations of magnetic nanoparticles in biocomposites. Mater Chem Phys 2017;193:364–70.
36. Krishnan KM. Fundamentals and Applications of Magnetic Materials. Oxford, UK: Oxford University Press; 2016.
37. Hoell A, Muller R, Heinemann A, Wiedenmann A. Structure investigations of barium hexaferrite ferrofluids and their precursors by sans with polarized neutrons. Magnetohydrodynamics 2003; 39:111–18.

38. Darbandi M, Stromberg F, Landers J, Reckers N, Sanyal B, Keune W, et al. Nanoscale size effect on surface spin canting in iron oxide nanoparticles synthesized by the microemulsion method. J Phys Appl Phys 2012;45:195001.
39. Landers J, Stromberg F, Darbandi M, Schöppner C, Keune W, Wende H. Correlation of superparamagnetic relaxation with magnetic dipole interaction in capped iron-oxide nanoparticles. J Phys Condens Matter 2014;27: 026002.
40. Cell experiments for biocompatibility studies were carried out by Dr. J. Clement, Department Hematology/Oncology, University Hospital of Jena. Germany: Friedrich-Schiller University of Jena. 07747.
41. Investigations on the biodegradation of the bionanocomposites in artificial body fluids were carried out by Prof. Dr. D. Fischer, Department of Pharmaceutical Technology and Biopharmacy. Germany: Friedrich-Schiller University of Jena. 07743Germany.
42. Heinze T, Müller R, Zhou M, Rabel M, Warncke P, Fischer D. Studies on the controlled release of drugs from magnetic nanobiocomposites. IJFAC 2019;4:1–8.
43. Gutiérrez L, Romero S, da Silva GB, Costo R, Vargas MD, Ronconi CM, et al. Degradation of magnetic nanoparticles mimicking lysosomal conditions followed by AC susceptibility. Biomed Eng/ Biomedizinische Technik 2015;60:417–25.
44. Hilger I. In vivo applications of magnetic nanoparticle hyperthermia. Int J Hyperther 2013;29: 828–34.
45. Müller R, Zhou M, Liebert T, Dellith A, Dutz S, Borin D, et al Performance analysis of carrier-less modulation schemes for wireless nanosensor networks. In: IEEE Proceedings of the 15th International Conference on Nanotechnology (IEEE-NANO) Rome, Italy: IEEE-NANO); 2015. p. 1–4. https://doi.org/10.1109/NANO.2015.7388731.